

## Mechanism of coherent acoustic phonon generation under nonequilibrium conditions

H. Park, X. Wang, S. Nie, R. Clinite, and J. Cao

*Physics Department and National High Magnetic Field Laboratory, Florida State University, Tallahassee, Florida 32310, USA*

(Received 17 June 2005; published 12 September 2005)

We have investigated the dynamics of coherent acoustic phonons generated with ultrafast optical excitation in monoatomic Al films using femtosecond electron diffraction. Associated coherent and thermal lattice motions were measured simultaneously with sub milli-ångström spatial resolution in real time. We show here that the phonon dynamics can be well fitted with a classical harmonic oscillator model using a driving force which includes both electronic and lattice contributions. In particular, the pressure of hot free electrons contributes significantly in driving the coherent acoustic phonons under nonequilibrium conditions when electrons and phonons are not thermalized.

DOI: [10.1103/PhysRevB.72.100301](https://doi.org/10.1103/PhysRevB.72.100301)

PACS number(s): 63.20.Kr, 07.78.+s, 78.47.+p

Coherent phonons in solids can be generated by impulsive optical excitation and their generating mechanisms have been studied extensively. In transparent media, coherent optical phonons are initiated via impulsive stimulated Raman scattering (ISRS).<sup>1,2</sup> In absorbing materials, several mechanisms have been proposed, including displacive excitation of coherent phonons<sup>3,4</sup> (DECP) and, more recently, resonant ISRS.<sup>5</sup> For coherent acoustic phonons, besides direct optical excitation of the zone-folded acoustic branch in semiconductor super lattice,<sup>6</sup> the most widely used generation scheme is through ultrafast heating of thin films<sup>7</sup> and nanoparticles.<sup>8-10</sup> In these cases associated acoustic phonons are standing waves with phonon period proportional to the particle radius or film thickness. Previously, optical pump-probe studies<sup>8,11,12</sup> of acoustic phonons generated via ultrafast heating indicate that the electron pressure might play an important role in driving coherent acoustic phonons. However, quantitative and direct measurements of the contributions of electron and lattice heating in driving coherent acoustic phonons have, to date, remained elusive.

Here we report the study of coherent acoustic phonon dynamics by directly measuring the associated structural changes in real time with femtosecond electron diffraction (FED). The damped single-mode breathing motion of an Al film along the surface normal was recorded as the coherent oscillation of Bragg peak positions. The concurrent lattice temperature evolution (transient driving force) was measured by following the associated intensity attenuation of the Bragg peaks. These data were fitted with the differential equation of a damped harmonic oscillator driven by both lattice and electron heating. The results show that the pressure of hot free electrons contributes significantly as a driving force under the conditions that electrons and phonons have not reached their thermal equilibrium.

The coherent acoustic phonons associated with a single-mode one-dimensional (1D) standing wave were generated by fs optical excitation of a thin polycrystalline Al film.<sup>13</sup> The thin-film samples were prepared by thermal evaporation of Al in high vacuum on freshly cleaved NaCl single-crystal substrates, then detached in a solvent and transferred to TEM grids as freestanding films. A film thickness of  $20 \pm 3.0$  nm was measured during evaporation with a quartz crystal thickness monitor. The pump laser pulses, with wavelength cen-

tered at 790-nm and 50-fs temporal duration, were focused down to a  $\sim 2$  mm spot on the film surface at an incident angle less than  $10^\circ$ . After the absorption of optical pulses, an expanded equilibrium lattice position was established from the nearly uniform and ultrafast heating of thin film,<sup>18</sup> thus causing a highly stressed state in a timescale faster than the lattice can respond. Consequently, a coherent lattice vibration centered at the equilibrium position was launched in the form of acoustic waves.<sup>8,11-15</sup> Since the linear dimension of the excitation laser beam ( $\sim 2$  mm) is much larger than the film thickness, this lattice motion can be treated as one-dimensional along the direction of surface normal with open-end boundary conditions (freestanding film). This leads to the creation of a 1D longitudinal standing sound wave (a breathing motion along the surface normal) in the Al film with a vibration period of  $T=2L/\nu$ , where  $\nu$  is the longitudinal sound velocity of 6420 m/s.<sup>16</sup>

Structural dynamics associated with the coherent acoustic phonons were probed in real time with transmission femtosecond electron diffraction<sup>17</sup> inside a UHV chamber with a base pressure less than  $3 \times 10^{-10}$  torr. The probe electron beam with a diameter of 330  $\mu\text{m}$  was directed normal to and spatially overlapped with pump laser beam on the film surface. Delay times between the pump and probe pulses were controlled by varying their relative optical path length difference. To maintain optimal temporal resolution, the probe electron beam intensity was set very low; containing less than 1000  $e^-$ /pulse. The corresponding temporal pulse width was less than 400 fs as determined *in situ* with our streak camera.<sup>18</sup> The overall temporal resolution, convoluting the excitation laser pulse width, probe electron pulse width, and the temporal degradation, was less than 500 fs.<sup>18</sup> In the FED measurements, the laser excitation fluence was kept less than 3  $\text{mJ}/\text{cm}^2$  and no sample damage was observed even after extended exposure to pump laser pulses. Additionally, diffraction patterns without the pump laser were also recorded at each time delay and used as a reference for data analysis to correct any extraneous changes, such as probe electron beam walking and long-term system drift.

A typical diffraction intensity curve of freestanding thin film aluminum is shown in Fig. 1. This curve is obtained by radially averaging the corresponding 2D transmission dif-

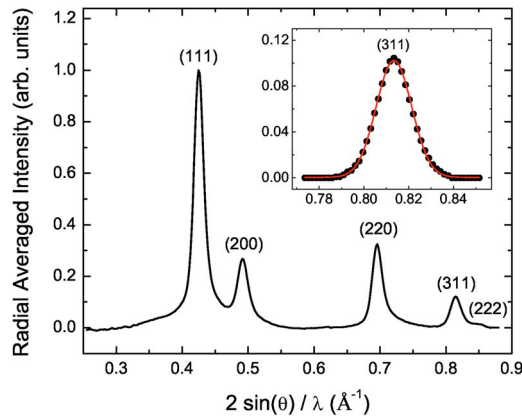


FIG. 1. (Color online) Diffraction intensity curve of freestanding thin film aluminum. Inset: A typical fit of (311) Bragg peak to a Gaussian profile. The peak center position was determined to be  $0.81669 \pm 0.00004$  ( $\text{\AA}^{-1}$ ) ( $470.99 \pm 0.02$  pixel).

fraction pattern, which was recorded with approximately  $2 \times 10^7$  probe electrons at an excitation laser fluence of  $2.3 \text{ mJ/cm}^2$ . To obtain a quantitative measurement of coherent lattice motions, each Bragg peak in an intensity curve was fitted with a Gaussian line profile to determine the peak center [see inset of Fig. 1 for Bragg (311) peak], which is defined as peak position. The relative peak position change was then calculated by dividing the data with the pump laser on by those with the pump beam blocked. This diffraction data processing scheme, combined with a superior signal-to-noise ratio, makes it possible to detect a change in relative Bragg peak position of less than 0.02%. This sensitivity corresponds to a spatial resolution less than a milli-ångström.<sup>13</sup>

The temporal evolution of (311) Bragg peak positions is shown in Fig. 2. After optical excitation, the peak starts its oscillation centered at a reduced Bragg ring radius (expanded equilibrium lattice constant). The vibration has a maximum displacement at time zero and displays nearly a cosine time dependence similar to the DECP excitation.<sup>3</sup> The corresponding Fourier transform of vibration data yields a single peak centered at 0.16 THz. The corresponding 6.3 ps vibrational period is in excellent agreement with the 1D standing wave condition  $T=2L/\nu$ , by using the nominal average film thickness ( $L$ ) of  $20 \pm 3.0$  nm and sound velocity of 6420 m/s. The temporal evolutions of all the other Bragg peak positions were also analyzed and found to oscillate perfectly in phase with one another with the same vibrational period.<sup>13</sup> This in-phase oscillation of all the Bragg peaks indicates that a single phonon mode correlated with the breathing motion along the surface normal was generated from nearly uniform heating of the film.<sup>13</sup>

To gain a complete picture of the lattice dynamics, we also measured the temporal evolution of lattice temperature  $T_l$  by monitoring the associated Bragg peak intensity attenuation as a function of pump-delay time, as displayed in Fig. 3. These data were obtained by first calculating the (311) peak intensity then normalizing to that of the (111) peak for each diffraction intensity curve at a given time delay. We then converted this normalized intensity to lattice temperature using the Debye-Waller factor<sup>19</sup> calibrated with the

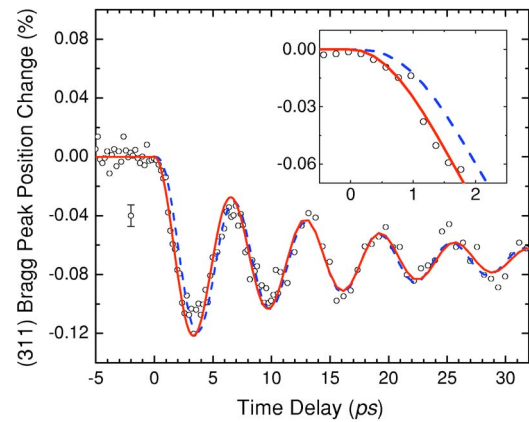


FIG. 2. (Color online) Temporal evolution of (311) Bragg peak positions. Positive time delays correspond to probe electron pulses arriving after excitation laser pulses. The error bar represents one standard deviation in the Gaussian peak profile fitting for determining the peak centers. The solid line is the fit to the experimental data using Eq. (2). The dashed curve is a fit excluding  $\sigma_e$ , which lags behind the data with a phase shift of approximately  $18^\circ$ . Inset: Detailed view of the above two fitting results in the range of  $-0.5$  to  $2.5$  ps.

static diffraction data by varying the film temperature in the range of 280 to 530 K. The time constant of  $\tau_{e-ph} = 600 \pm 100$  fs for lattice thermalization, together with the time-zero uncertainty of 90 fs, were extracted by fitting the data with an exponential function (solid line in Fig. 3). The corresponding lattice heating time of 1.8 ps is in excellent agreement with more recent studies of ultrafast heating of Al using transient optical reflectivity, where an approximately 2-ps time was observed.<sup>20,21</sup> Importantly, this 1.8 ps timescale is comparable to one quarter of the vibrational period. By this time the coherent lattice vibration has nearly reached its new equilibrium position with highest vibration speed. These observations clearly show that the two modes of lattice motions, namely coherent vibration and random thermal motions, are taking place concurrently after excitation.

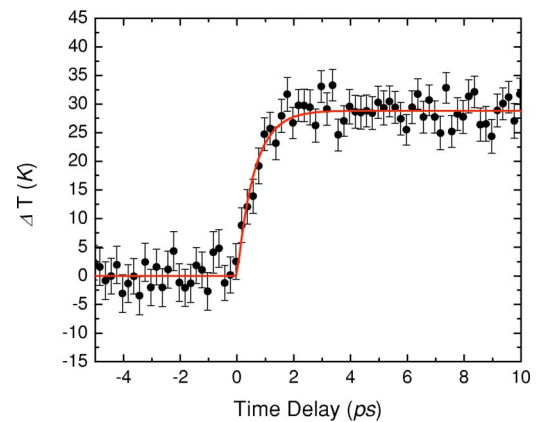


FIG. 3. (Color online) Temporal evolution of the lattice temperature. The solid line is a fit to the data using an exponential function. The time constant for lattice thermalization is determined to be  $600 \pm 100$  fs.

For a nonmagnetic metal, the stress responsible for thermal lattice expansion consists of two independent contributions: the thermal stress related to the lattice anharmonicity ( $\sigma_l$ ) and the thermal pressure from hot free electrons ( $\sigma_e$ ).<sup>22</sup> Assuming the electrons and phonons maintain separate states of equilibrium characterized by temperature deviations of  $\delta T_e$  and  $\delta T_l$ , the combined stress due to these two effects in absorbing solids excited with ultrashort optical pulses can be written as<sup>11,14,23,24</sup>

$$\sigma = \sigma_e + \sigma_l = -\gamma_e C_e \delta T_e - \gamma_l C_l \delta T_l, \quad (1)$$

where  $C_e$  and  $C_l$  are specific heat for electrons and phonons,  $\gamma_e$  and  $\gamma_l$  are the corresponding Grüneisen constants. Here the spatial dependence in  $\sigma$  can be dropped, considering that the thin film was nearly uniformly heated as described earlier. This leaves  $\sigma$  as a function of delay time only and solely determined by the temporal evolutions of electron and lattice temperatures. While the lattice contribution to stress dominates after the electron-lattice equilibrium at room temperature and above, the transient electron heating ( $T_e \geq 1200$  K) well above the lattice temperature could make the electrons contribute significantly to driving coherent lattice motion at short times. Under this nonequilibrium condition, the critical parameter is the ratio of lattice thermalization time ( $\sim 3\tau_{e-ph}$ ) over the quarter period  $T/4$  of coherent lattice vibration. If  $12\tau_{e-ph}/T \ll 1$ , the lattice contribution takes control of coherent motion. The fact that the coherent lattice oscillations were launched much earlier before reaching its thermal equilibrium with hot electrons implies that electron pressure might play a significant role in driving coherent lattice motion.

The roles of electron and lattice heating in driving the coherent acoustic phonons were analyzed by fitting the vibration data with the differential equation of a damped harmonic oscillator driven by both lattice and electron heating. For sufficiently small lattice vibrations in a single acoustic mode, the temporal evolution of the coherent phonon field  $Q$  (displacement of coherent lattice vibration) can be described by a classical simple harmonic oscillator as<sup>3,4</sup>

$$\frac{d^2 Q}{dt^2} + 2\beta \frac{dQ}{dt} + \omega_0^2 Q = C\sigma(t), \quad (2)$$

where  $\omega_0$  is the phonon angular frequency,  $\beta$  is a phenomenological damping constant, and  $C$  is a scaling factor used to match the magnitude of  $\sigma$  to the oscillation amplitude. Assuming that the total energy deposit into a unit volume ( $E_{total}$ ) by the optical pulse is conserved on the ps time span, we have  $C_e \delta T_e + C_l \delta T_l = E_{total} g(t)$ , where  $g(t)$  is a normalized function representing the temporal profile of the 50-fs pump pulse. Under this condition, the lattice heating can be expressed as  $C_l \delta T_l = E_{total} (1 - e^{-t/\tau_{e-ph}})$ . Accordingly, the temporal evolution of stress  $\sigma$  can be uniquely determined by the experimentally measured  $\tau_{e-ph}$  as

$$\begin{aligned} \sigma &= \sigma_e + \sigma_l \\ &= -\gamma_e E_{total} (g(t) - 1 + e^{-t/\tau_{e-ph}}) - \gamma_l E_{total} (1 - e^{-t/\tau_{e-ph}}). \end{aligned} \quad (3)$$

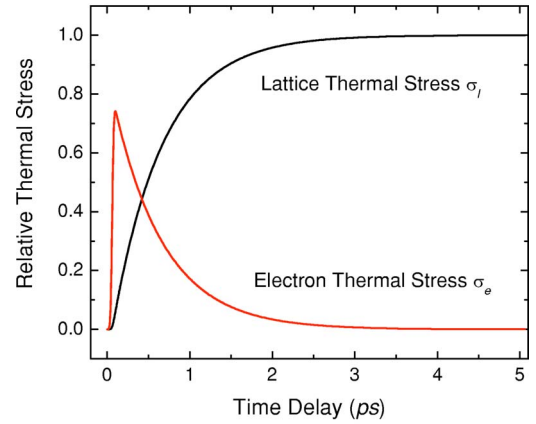


FIG. 4. (Color online) Temporal evolution of the stress from electron ( $\sigma_e$ ) and lattice ( $\sigma_l$ ) heating.

The solid curve in Fig. 2 displays the least-square fit of vibration data to a damped harmonic oscillator using Eqs. (2) and (3), and with values of  $\gamma_l = 2.16$ ,  $\gamma_e = 1.6$ .<sup>22</sup> In the fitting, the electron-phonon thermalization time constant ( $\tau_{e-ph} = 600 \pm 100$  fs) and time zero ( $t_0 = 0 \pm 90$  fs) were fixed to the values measured by FED, and the three other parameters,  $\omega_0$ ,  $\beta$ , and  $C$  were floated. The fitting result, with phonon angular frequency  $\omega_0 = 0.99 \pm 0.01$  THz and the damping constant  $1/\beta = 15 \pm 1$  ps, is in very good agreement with the coherent lattice vibration data. The fitted value of  $\omega_0$  is the same as that obtained with direct Fourier transform.

The transient stresses from the lattice and the electron heating obtained from the above data analysis are plotted in Fig 4.  $\sigma_l$  and  $\sigma_e$  have similar strengths but display different transient behaviors.  $\sigma_l$  exhibits a steplike temporal dependence, the same as that of  $\delta T_l$ , and determines the equilibrium lattice position; while  $\sigma_e$  displays a  $\delta$ -like function form and only plays a significant role in the early heating stage before electrons and phonons reach their thermal equilibrium. To quantitatively evaluate the role of electronic heating, we fitted the vibration data using only lattice heating as a driving force. The fitting results are shown as the dashed line in Fig. 2 with angular frequency  $\omega_0 = 1.01 \pm 0.01$  THz and the damping constant  $1/\beta = 16 \pm 1$  ps. While both models give good fits to the experimental data after 10 ps time delay, it is apparent that the fit which includes both  $\sigma_l$  and  $\sigma_e$  is significantly better than that excluding  $\sigma_e$  at early times before 10 ps. In particular, the latter creates a significant phase lag of approximately  $18 \pm 5^\circ$  with respect to the vibration data (inset of Fig. 2). These results provide direct and unambiguous evidence that electronic thermal expansion is essential to drive coherent acoustic phonons, and plays a significant role for the first quarter cycle of lattice vibration.

In summary, we have measured in real time the transiently generated structural dynamics in Al films with sub milliangström spatial resolution using femtosecond electron diffraction. This study is different from previous experiments<sup>8,11,12,14</sup> in that both coherent and thermal lattice motions were directly measured and differentiated. In particular, quantitative analysis using a classical harmonic oscillator model provides direct and unambiguous evidence that

the pressure of hot electrons contributes significantly in driving coherent acoustic phonons.

We thank Dr. P. Xiong and Dr. S. von Molnár for the use of their thin-film preparation equipment. We are also

grateful to Dr. P. Schlottmann for helpful discussion and for carefully reading the manuscript. This work was supported by the Florida State University and the National Science Foundation by Grant No. DMR-0305519.

- 
- <sup>1</sup>Y. X. Yan, E. B. Gamble, and K. A. Nelson, *J. Chem. Phys.* **83**, 5391 (1985).
- <sup>2</sup>Y. X. Yan and K. A. Nelson, *J. Chem. Phys.* **87**, 6240 (1987).
- <sup>3</sup>H. J. Zeiger, J. Vidal, T. K. Cheng, E. P. Ippen, G. Dresselhaus, and M. S. Dresselhaus, *Phys. Rev. B* **45**, 768 (1992).
- <sup>4</sup>A. V. Kuznetsov and C. J. Stanton, *Phys. Rev. Lett.* **73**, 3243 (1994).
- <sup>5</sup>G. A. Garrett, T. F. Albrecht, J. F. Whitaker, and R. Merlin, *Phys. Rev. Lett.* **77**, 3661 (1996).
- <sup>6</sup>A. Yamamoto, T. Mishina, Y. Masumoto, and M. Nakayama, *Phys. Rev. Lett.* **73**, 740 (1994).
- <sup>7</sup>C. Thomsen, J. Strait, Z. Vardeny, H. J. Maris, J. Tauc, and J. J. Hauser, *Phys. Rev. Lett.* **53**, 989 (1984).
- <sup>8</sup>M. Nisoli, S. DeSilvestri, A. Cavalleri, A. M. Malvezzi, A. Stella, G. Lanzani, P. Cheyssac, and R. Kofman, *Phys. Rev. B* **55**, R13424 (1997).
- <sup>9</sup>T. D. Krauss and F. W. Wise, *Phys. Rev. Lett.* **79**, 5102 (1997).
- <sup>10</sup>G. V. Hartland, *J. Chem. Phys.* **116**, 8048 (2002).
- <sup>11</sup>G. Tas and H. J. Maris, *Phys. Rev. B* **49**, 15046 (1994).
- <sup>12</sup>M. Perner, S. Gresillon, J. Marz, G. von Plessen, J. Feldmann, J. Porstendorfer, K. J. Berg, and G. Berg, *Phys. Rev. Lett.* **85**, 792 (2000).
- <sup>13</sup>H. Park, S. Nie, X. Wang, R. Clinite, and J. Cao, *J. Phys. Chem. B* **109**, 13854 (2005).
- <sup>14</sup>A. M. Lindenberg, I. Kang, S. L. Johnson, T. Missalla, P. A. Heimann, Z. Chang, J. Larsson, P. H. Bucksbaum, H. C. Kapteyn, H. A. Padmore, R. W. Lee, J. S. Wark, and R. W. Falcone, *Phys. Rev. Lett.* **84**, 111 (2000).
- <sup>15</sup>A. Cavalleri, C. W. Siders, F. L. H. Brown, D. M. Leitner, C. Toth, J. A. Squier, C. P. J. Barty, K. R. Wilson, K. Sokolowski-Tinten, M. H. von Hoegen, D. von der Linde, and M. Kammler, *Phys. Rev. Lett.* **85**, 586 (2000).
- <sup>16</sup>*CRC Handbook of Chemistry and Physics*, 82nd ed. edited by D. R. Lide, (Chemical Rubber Company, Roca Raton, Florida, 2002).
- <sup>17</sup>J. Cao, Z. Hao, H. Park, C. Tao, D. Kau, and L. Blaszczyk, *Appl. Phys. Lett.* **83**, 1044 (2003).
- <sup>18</sup>H. Park, S. Nie, X. Wang, R. Clinite, and J. Cao, *Solid State Commun.* (to be published).
- <sup>19</sup>L. Reimer, *Transmission Electron Diffraction*, 4th ed. (Springer-Verlag, New York, 1997).
- <sup>20</sup>J. L. Hostetler, A. N. Smith, D. M. Czajkowsky, and P. M. Norris, *Appl. Opt.* **38**, 3614 (1999).
- <sup>21</sup>C. J. K. Richardson and J. B. Spicer, *Appl. Phys. Lett.* **80**, 2895-2897 (2002).
- <sup>22</sup>T. H. K. Barron, J. G. Collins, and G. K. White, *Adv. Phys.* **29**, 609 (1980).
- <sup>23</sup>C. Thomsen, H. T. Grahn, H. J. Maris, and J. Tauc, *Phys. Rev. B* **34**, 4129 (1986).
- <sup>24</sup>O. B. Wright, *Phys. Rev. B* **49**, 9985 (1994).